Chapter 4
The Arterial System I. Pressure, Flow and Stiffness

Peter R. Hoskins and D. Rodney Hose

Learning outcomes

1. Describe the main constituents of an artery.
2. Describe the organisation of elastin and collagen in the artery.
3. Describe the stress–strain (pressure–diameter) behaviour of arteries.
4. Discuss the stress–strain behaviour of arteries in terms of the mechanical properties of elastin and collagen.
5. Describe pressure–time and velocity-flow waveforms in different arteries.
6. Describe the Windkessel model.
7. Discuss how the Windkessel model produces velocity–time and pressure–time waveforms.
8. Describe pressure wave propagation.
9. Define the Moens–Korteweg equation for pressure wave velocity.
10. Discuss how pressure–time and velocity–time waveforms in arteries arise from pressure wave propagation and reflected waves.
11. Describe laminar, turbulent and disturbed flow in arteries.
12. Describe axial and rotating flow in arteries.
13. Discuss fully developed flow and non-fully developed flow in arteries.

This chapter will explore basic biomechanics of arteries concentrating on pressure, flow and stiffness. Here the emphasis will be on normal function. Abnormal function and disease will be considered in later chapters. In the appendix at the end of the chapter is a table of the values of key quantities in different arteries.

P.R. Hoskins (✉)
Edinburgh University, Edinburgh, UK
e-mail: P.Hoskins@ed.ac.uk

D.R. Hose
Sheffield University, Sheffield, UK

P.R. Hoskins et al. (eds.), *Cardiovascular Biomechanics*,
DOI 10.1007/978-3-319-46407-7_4

4.1 Stiffness of Arteries

This section describes the stiffness and stress–strain behaviour of arteries in relation to their biological composition.

4.1.1 Structure and Composition of Arteries

Figure 4.1 shows the main structures present within an artery. The endothelium, the basement membrane and the internal elastic lamina (a thin sheet of elastin) together make up the intima on which endothelial cells are attached. The internal elastic membrane allows the endothelium to move independently of the media. The media contains elastin fibres which provide elasticity, collagen fibres which provide strength, and smooth muscle cells. The outermost layer is the adventitia which contains mainly collagen fibres.

From a mechanical point of view the two most important constituents of arteries are collagen and elastin. These are arranged in layers around the artery. The number of sheets increases during gestation but is fixed at birth. The molecules are arranged in a helical pattern around the artery, with a different pitch for different layers within the artery. The collagen molecules are present in a loose, wavy network in the adventitia. As the artery expands so the molecules unfurl to reach their straightened lengths at which point they become extremely stiff. This behaviour protects the smooth muscle cells from acute over-distension.

Elastin is a stable protein with a long half-life of around 50 years, so that the elastin sheets laid down in early life remain in place into later life. Collagen, on the other hand, has a half-life of 2 weeks, and thus is in a continuous state of turnover.

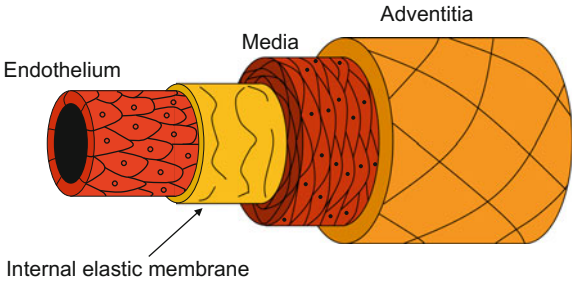

Fig. 4.1 The main components of an artery

4.1.2 *Stress–Strain Behaviour in Arteries*

The stress–strain behaviour of an artery may be characterised by a plot of pressure versus diameter. Figure 4.2 shows pressure–diameter behaviour in an excised artery subject to an inflation pressure. The diameter-pressure behaviour is nonlinear, though over a restricted range (e.g. 80–120 mmHg) it is approximately linear. Within the physiologic range Fig. 4.2 shows a 10 % increase in diameter which is typical of the variation found in vivo during the cardiac cycle.

The contribution of elastin and collagen to the stress–strain behaviour was explored by Roach and Burton (1957). Figure 4.3 shows the tension-radius behaviour for 3 samples of artery. In the left curve the elastin has been removed by a chemical process so that the mechanical behaviour of the artery is governed by the collagen. The artery is quite stiff so that high stress has to be provided to stretch the vessel. In the right trace the collagen has been digested so that mechanical

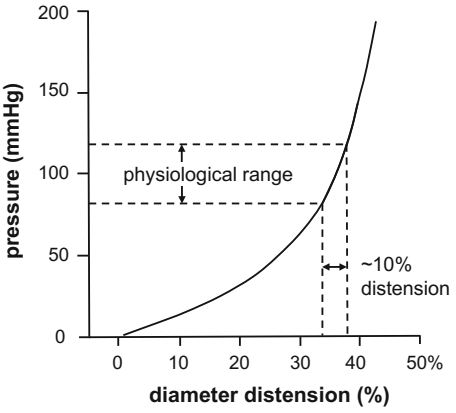

Fig. 4.2 Pressure-distension for an artery. The behaviour is nonlinear; the physiologic range of 80–120 mm Hg produces a 10 % variation in diameter

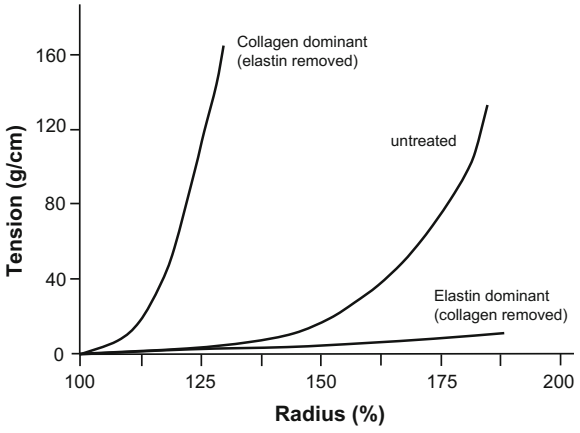

Fig. 4.3 Effect of collagen and elastin on the tension-radius behaviour for an artery. Removal of elastin leads to stiffening; removal of collagen leads to more elastic behaviour. From: Roach MR, Burton AC; The reason for the shape of the distensibility curve of arteries; Can J Biochem Physiol. 1957;35:681–690; © Canadian Science Publishing or its licensors; redrawn with permission

behaviour is governed by the elastin. The artery is now quite elastic so that that small changes in stress result in large changes in diameter. The elastic behaviour of the untreated artery can be explained by the different behaviours of collagen and elastin. At small distensions the collagen fibres are quite crimped and the behaviour is dominated by elastin. At high extensions the collagen fibres have straightened out; these now dominate mechanical behaviour and the artery becomes very stiff. This may be likened to a balloon in a net. Blowing up the balloon is easy until it is the same size as the net, at which point it is difficult to blow up the balloon much further.

As introduced in Chap. 1, the elastic modulus of elastin, collagen and arteries may be measured in a tensile testing system. The elastic modulus for elastin is low at 0.4–0.6 MPa but for collagen is much higher at 100 MPa. Arteries have intermediate values of 1–5 MPa (Ryan and Foster 1997). Note that, in the case of collagen and artery, incremental elastic modulus values are reported as the stress–strain behaviour is nonlinear. The Young's modulus for an artery describes the composite behaviour.

The artery is a multi-layer structure and each layer has different mechanical properties. However to describe the overall stress–strain or diameter–pressure behaviour for an artery it is not necessary to know the elastic moduli of the different layers. This approach assumes that the artery is uniform and homogeneous; i.e. that the wall thickness and elastic composition are the same for different positions around the circumference. This assumption is valid in healthy arteries although it may not be true in disease due to 3D changes in geometry, wall thickness and wall composition (see later chapters).

4.2 Pressure and Flow Waveforms in Arteries

Figure 4.4 shows pressure–time waveforms from various arteries in the systemic circulation. The baseline or diastolic pressure in this example is about 80 mm Hg. The peak or systolic pressure increases with distance from the heart; in this example from 110 mm Hg at the aortic outflow to 160 mm Hg at the tibial arteries. There is also some change in shape of the pressure waveform with distance from the heart. Figure 4.4 also shows velocity–time waveforms taken using Doppler ultrasound. The waveforms are all similar in that they have a period of forward flow followed by a period of reverse flow. Figure 4.5 shows more time–velocity waveforms, taken from arteries supplying the brain and kidney. These organs have a low vascular resistance and the time–velocity waveforms have flow throughout the cardiac cycle. In this section we will be looking at the origins of the shape of the pressure and flow waveforms in different arteries.

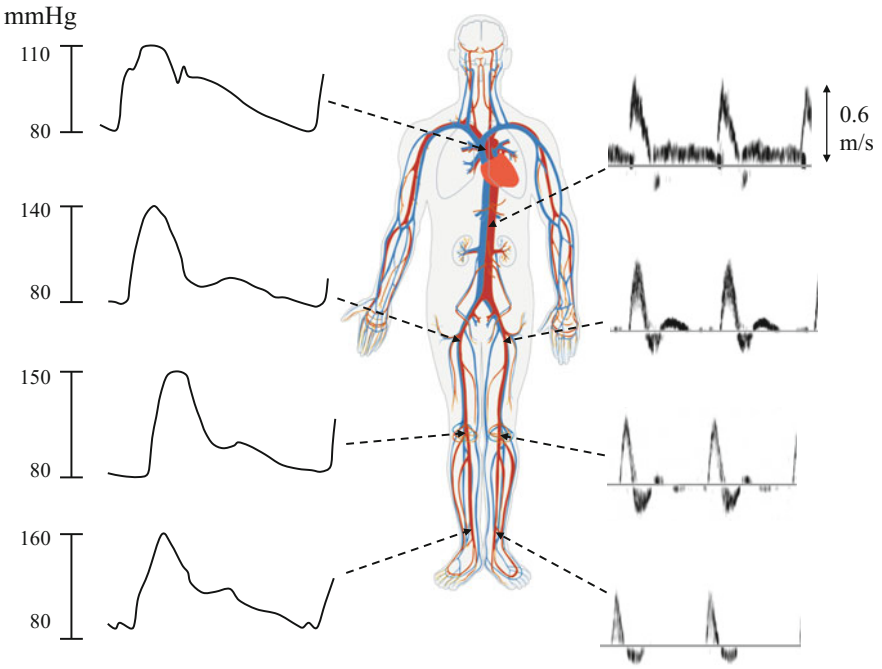

Fig. 4.4 Blood pressure–time and velocity–time waveforms at increasing distance from the heart. There is a baseline (diastolic) pressure of 80 mm Hg; the peak (systolic) pressure increases with distance and there are changes in the overall shape. The flow waveforms are taken from Doppler ultrasound. The waveforms are pulsatile with a period of forward flow followed by a period of reverse flow then more forward flow. Circulation figure reproduced from Wikipedia; https://commons.wikimedia.org/wiki/File:Circulatory_System_en.svg. This image is in the public domain and was authored by Mariana Ruiz Villarreal

4.2.1 Windkessel Model

Models of pressure and flow in the arterial system generally only consider the arteries. The pressure at the capillaries (as noted in Chap. 2) is a fixed value close to zero so the venous system does not need to be taken into account when modelling the arterial system. An early model which tried to explain the pressure–time and flow-time waveforms is the Windkessel model. This comes from the German word 'Windkessel' meaning 'air chamber'. The Windkessel model of the systemic circulation consists of three elements (Fig. 4.6); a pump representing the heart, an elastic chamber representing the arteries, and an outflow resistance representing flow through the arterioles. The process can be broken into 3 phases:

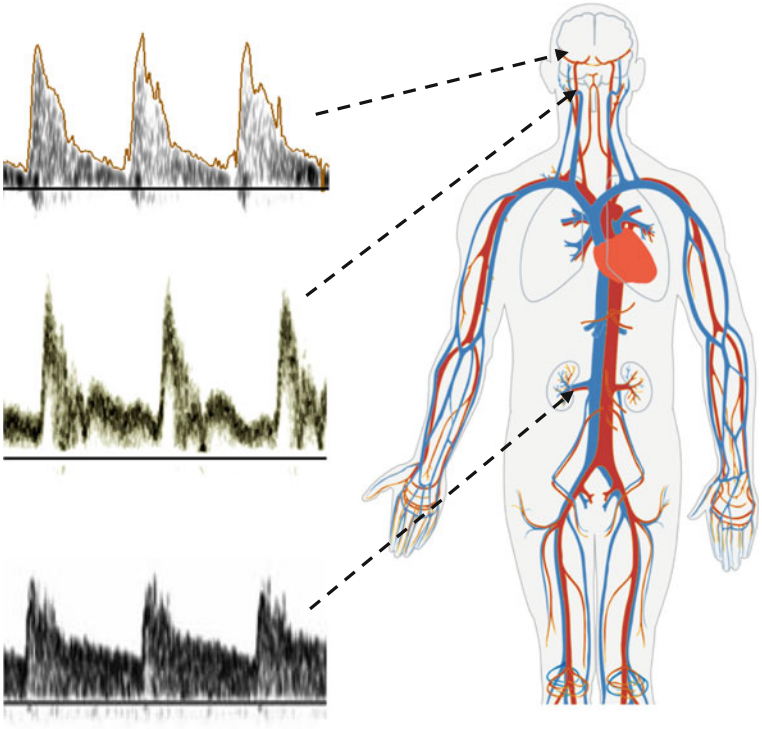

Fig. 4.5 Velocity–time waveforms from arteries supplying organs (brain and kidney) with high metabolic demand. Waveforms demonstrate a high baseline of flow. Circulation figure reproduced from Wikipedia; https://commons.wikimedia.org/wiki/File:Circulatory_System_en.svg. This image is in the public domain and was authored by Mariana Ruiz Villarreal

- *Ejection phase*. The heart contracts ejecting blood into the compliant chamber. The ejection takes about 100 ms. The tension in the wall of the chamber causes a pressure on the blood, which is forced out through the resistance vessels. Pressure and flow reach a maximum at the end of the ejection phase.
- *Relaxation phase*. The ejection of blood from the heart stops. This is the relaxation phase. As the chamber gradually returns to its resting position the pressure on the blood decreases. As a result of the decrease in pressure, the flow also reduces.
- *Resting phase*. The chamber returns to its resting position. This is the completion of the relaxation phase. The pressure reduces to its resting value and the flow reduces to zero.

There are some similarities between the pressure waveforms from the Windkessel model and those seen in Fig. 4.4, in that pressure reaches a peak and gradually reduces. The Windkessel flow waveforms also have a peak and gradually reduce in value thereafter, similar to those in Fig. 4.5 for arteries supplying brain

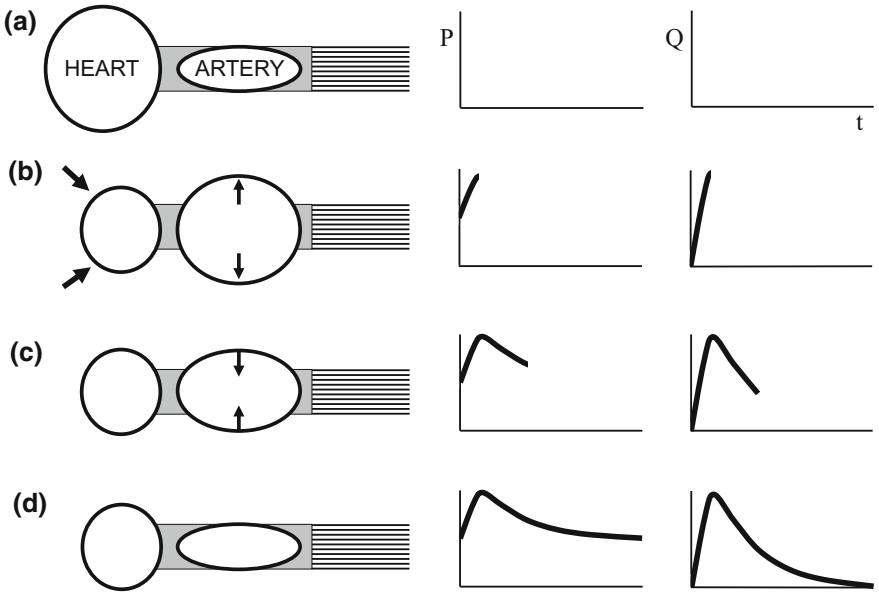

Fig. 4.6 Windkessel model consisting of a pump (heart), an elastic chamber (artery) and an outflow resistance (arteriolar bed). **a** Pre-ejection phase where the heart is full of blood. **b** In the ejection phase the heart contracts ejecting blood into the compliant chamber. The ejection takes about 100 ms. The tension in the wall of the chamber causes a pressure on the blood, which is forced out through the resistance vessels. Pressure and flow reach a maximum at the end of the ejection phase. **c** The ejection of blood from the heart stops. This is the relaxation phase. As the chamber gradually returns to its resting position the pressure on the blood decreases. As a result of the decrease in pressure, the flow also reduces. **d** The chamber returns to its resting position. The pressure reduces to its resting value and the flow reduces to zero

and kidney. However, the Windkessel flow waveforms bear little resemblance to the flow waveforms seen in Fig. 4.4 which have a period of reverse flow.

4.2.2 Wave Propagation Model

The Windkessel model is useful in basic understanding but it omits a key feature of the arterial system which is wave propagation. Ejection of blood from the left ventricle leads to expansion of the aorta in order to accommodate the ejected volume. The increase in circumference leads to an increase in tension within the arterial wall and hence an increase in pressure within the blood. The pressure passes down the artery in the form of a wave. This phenomenon can be demonstrated by recording the pressure with time at various locations from the heart. Figure 4.7

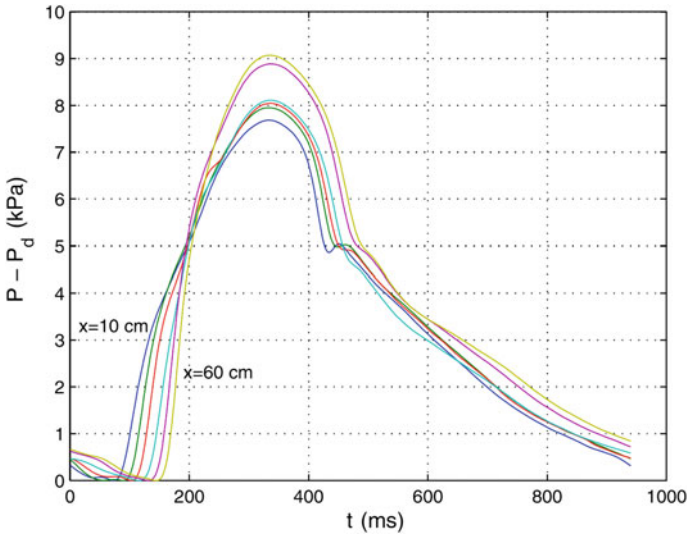

Fig. 4.7 Aortic pressure measured 10, 20, 30, 40, 50 and 60 cm downstream from the aortic valve plotted on as a function of time at different distances. The increase in pressure at the beginning of the waveform occurs at increasingly later times with distance demonstrating that the pressure propagates as a wave down the arterial tree. From Medical and Biological Engineering and Computing, An introduction to wave intensity analysis, Vol. 47, 2009, pp. 175–180, Parker KH, © International Federation for Medical and Biological Engineering 2009, with permission of Springer

shows the pressure–time waveform at different distances from the heart up to 60 cm. The increase in pressure at the beginning of the waveform occurs at later times. This is consistent with the idea that the pressure pulse propagates down the artery as a wave. The pressure wave propagation speed is usually called the 'pulse wave velocity' or PWV. The typical PWV in the thoracic aorta is about 5 m s^{-1} and increases, with distance from the heart, to about 15 m s^{-1} in the arteries of the lower leg. An important point is that pressure wave speed is not the same as blood speed. The pressure wave speed is the speed at which the pressure wave propagates and is typically 5–15 m s^{-1}. The blood speed is the speed at which the blood moves which is typically 0–1 m s^{-1} in health.

An early attempt to formulate an equation for PWV was made in 1878 by Moens and Korteweg. This states that PWV is related to the elastic modulus E of the artery, the wall thickness h, the diameter d and the density ρ of blood. This simple equation in practice predicts the correct PWV to within about 10 % in healthy arteries.

$$\mathrm{PWV} = \sqrt{\frac{Eh}{d\rho}} \tag{4.1}$$

4.2.3 *Propagation Model with Reflected Waves*

For propagation of any wave, in any medium, the wave will be scattered or reflected where there is a change in local impedance and this is also true for pressure waves in arteries. A change in impedance occurs as a result of change in diameter, shape or elastic properties. Common sites of reflected waves are at bifurcations; that is when a single parent artery splits into 2 or more daughter arteries. However, by far the largest contribution to reflected waves comes from the change in impedance which occurs between arteries and arterioles. The pressure–time waveform at a particular location in an artery is therefore a composite of the forward-going pressure wave, and a reverse-going pressure wave arising from downstream reflections at the level of the arterioles (Fig. 4.8a). The flow-time waveform can be considered in the same manner as a combination of a forward-going flow wave and a reverse-going flow wave (see e.g. Murgo et al. 1981). However, the flow waves combine in a subtractive manner (Fig. 4.8b). In the example shown in Fig. 4.8b the composite flow waveform has a period of reverse flow, similar to that seen in Fig. 4.4.

A simple model can help explain these features in more detail (Fig. 4.9). The components of the model are the heart, a block representing the large arteries, a

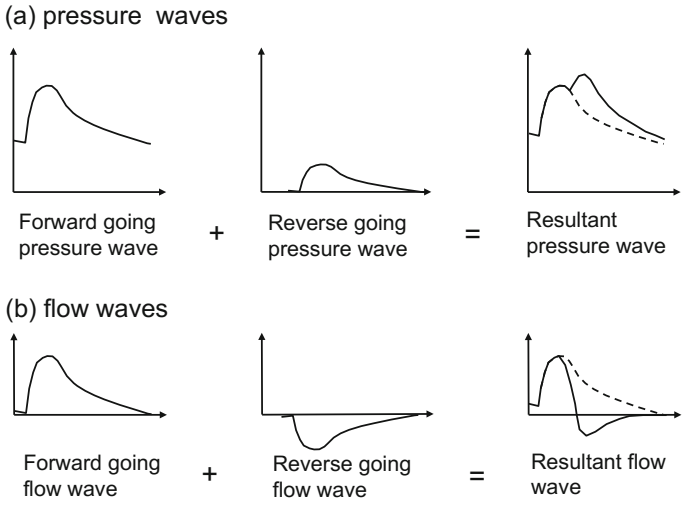

Fig. 4.8 Pressure and flow as a composite of forward-going waves and reverse-going waves; reverse waves are due to reflections, mainly from the distal arteriolar bed. **a** Forward and reverse pressure waves combine in an additive manner, producing an increase in maximum pressure. **b** Forward and reverse flow waves combine in a subtractive manner, in this case producing a period of reverse flow

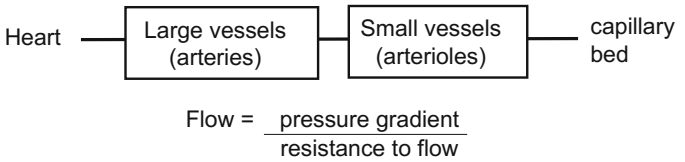

Fig. 4.9 A simple model of flow in arteries. The heart pumps blood through large vessels (arteries) and small vessels (arterioles) to the capillary bed. The large and mall arteries each has a resistance to flow. The overall flow rate is the ratio of the pressure gradient divided by the resistance to flow

block representing the arterioles, with a fixed value of pressure (22 mm Hg) at the level of the capillaries. The flow rate of blood is determined by the overall pressure difference between the heart and the capillaries and by the overall resistance to flow. The overall resistance to flow is the sum of the resistance in the arteries and the arterioles. In practice it is the arteriolar resistance which is used to control the flow rate. The arterioles are lined with smooth muscle which can constrict the diameter of the arterioles to create high resistance, such as may occur for muscles at rest which have low metabolic demands. When metabolic demands are high and a high flow rate is needed the smooth muscle in the arterioles relaxes, the diameter increases and the resistance drops. Local changes in flow rate are effected in the first instance by this mechanism, followed by associated increase in cardiac output. This then explains the features of flow waveforms seen in Figs. 4.4 and 4.5. In Fig. 4.4 the arteries are mostly supplying the buttocks and lower limbs. Since the bulk of this tissue is muscle at rest, the arteriolar resistance is high, the amplitude of reflected waves is high, and there is a large reverse flow component. In Fig. 4.5 the arteries are supplying the brain and the kidney which have high metabolic demand. The arteriolar resistance is low, the amplitude of reflected waves from the arteriolar bed is low and the flow is mainly dominated by the forward flow wave which has a high baseline of flow.

The above changes can be illustrated using a simple experiment; reactive hyperaemia in the arm (Fig. 4.10). In this example the hand is clenched while monitoring the flow in the brachial artery. During hand clenching blood is expelled from the hand and fingers. Metabolic demand build up and arterioles dilate but flow is unable to increase due to pressure constriction from the clenching. On release of the fist there is no pressure constriction and there is a sudden increase in flow rate due to arteriolar dilation. After unclenching the reverse flow waves have small amplitude and there is a large baseline of flow. Over 30–60 s the metabolic demands of the tissues are met and the flow waveform gradually returns to its resting state. During this time the arterioles become more constricted; the resistance in the arteriolar bed gradually increases, the amplitude of reverse-going waves

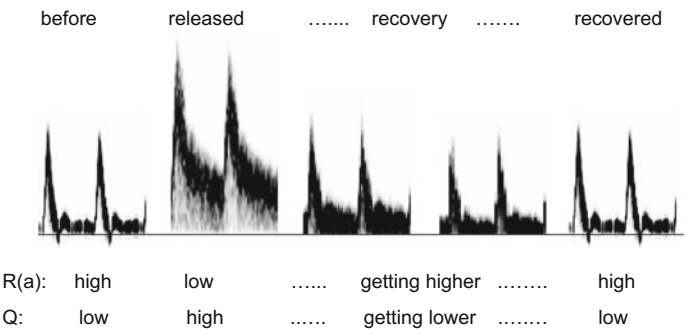

Fig. 4.10 Relationship between distal resistance and waveform shape illustrated by reactive hyperaemia. Doppler velocity–time waveforms are shown in the brachial artery. The hand is clenched for 2–3 min to increase metabolic activity. Clenching causes local compression; during clenching arterioles fully dilate but without increase in flow. On release of the hand there is a dramatic decrease in overall resistance leading to a huge increase in flow rate. The reflected waves have low amplitude and the velocity–time waveforms demonstrate flow throughout the cardiac cycle. During the recovery phase the arteriolar resistance increases, flow is reduced and the velocity–time waveforms become more pulsatile returning to a normal shape with reverse flow after 1–2 min

increases and eventually the baseline of flow is lost with return of the reverse flow component.

4.2.4 Pressure and Flow Waveforms at Different Distances from the Heart

With increasing distance from the heart, pressure waveforms in arteries change shape. In young adults there is increase in the pulse-pressure (systolic-diastolic) with distance from the heart (Nichols et al. 1993). This is seen in Fig. 4.4 where the peak pressure increases from 110 mm Hg in the ascending aorta to 160 mm Hg in the posterior tibial artery. Increase in pulse-pressure arises from increase in stiffness of arteries with increasing distance from the heart. This phenomenon continues down to very small arteries. Figure 4.11 shows increase in pulse-pressure from the brachial artery (3–4 mm diameter in the arm) to the digital artery (1–1.2 mm diameter in the finger).

For peak flow, velocity invasive measurements demonstrate decrease in peak velocity with distance from the heart (McDonald 1974). Peak velocity is easy to measure using Doppler ultrasound and Fig. 4.4 shows velocity–time waveforms from mid-aorta to the posterior tibial artery.

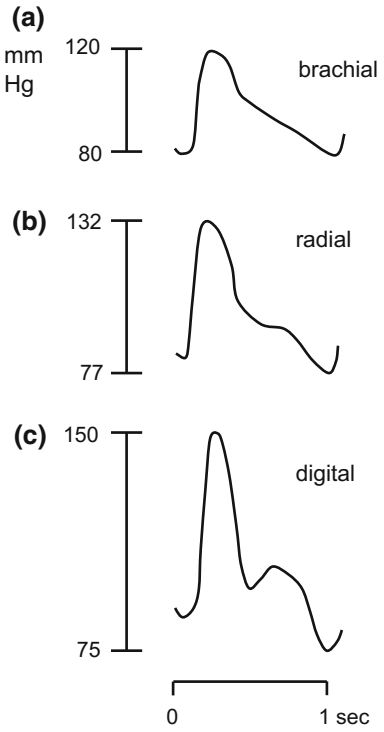

Fig. 4.11 Pressure–time waveforms from arteries in the arm and hand showing pressure augmentation in small arteries; **a** brachial, **b** radial, **c** digital

4.3 Flow in Arteries

This section discusses characteristics of the flow-field, i.e. the local 3D distribution of blood velocities, within arteries.

4.3.1 Turbulence, Disturbed and Laminar Flow

The principal flow characteristics of laminar and turbulent flow are determined by the Reynolds number. In the arterial system the mean Reynolds number decreases with distance from the heart. The highest Reynolds numbers are seen in the aorta, mainly in the systolic phase where values greater than 2000 regularly occur in the ascending aorta. This leads to periods of turbulent flow in the post-systolic phase of the flow waveform (Nerem et al. 1972). In the remainder of the arterial circulation in healthy individuals flow is laminar. In addition to laminar and turbulent flow it is useful to define a third flow state called ‘disturbed flow’ which relates to vortices and vortex shedding. Vortices or eddies are regions of circulating flow. These typically occur in the low shear region downstream of obstructions and are a

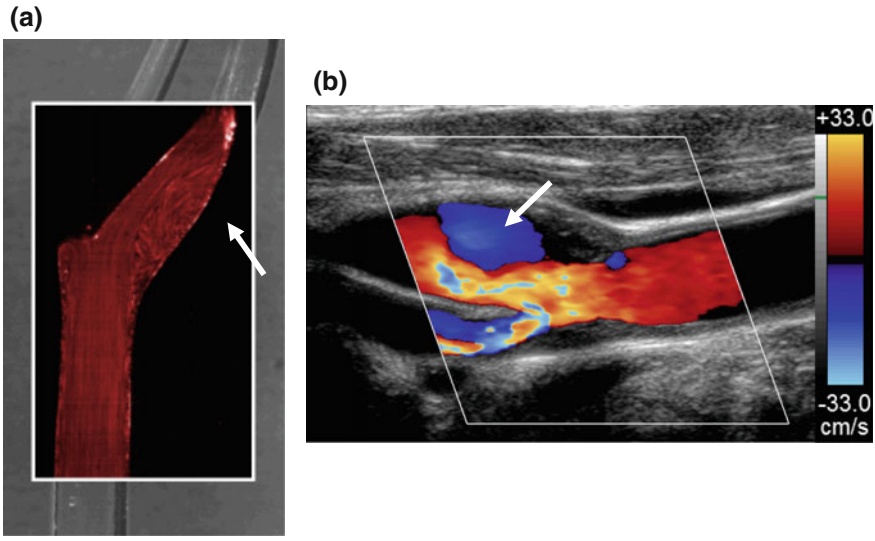

Fig. 4.12 Recirculation of flow in the carotid bulb. **a** An anatomical model of the carotid bifurcation with flow visualisation. **b** Colour flow ultrasound with recirculation shown in blue

common feature of vessel disease. They can also occur in healthy vessels and the one place where they are regularly seen is in the carotid sinus (Fig. 4.12). This is a dilated region at the entrance to the internal carotid artery and is associated with the location of sensors which monitor blood pressure in the body. Disturbed flow may also be seen in aneurysms, which are pathological bulges which can affect both the cerebral circulation and the aorta.

4.3.2 Rotating Versus Axial Flow

Flow in a long straight pipe will become axial after a certain distance, no matter what the flow conditions at the inlet. Rotation of flow is induced in a curved pipe and in the daughter arms of branching tubes. Though these phenomena are well known in fluid mechanics, evidence for rotation of flow in arteries only arose in the 1990s using both ultrasound and MRI (Kilner et al. 1993; Hoskins et al. 1994). Curvature and bifurcations in arteries will induce rotational flow; the fluid at the centre of the flow moves to the outer curve returning along the wall to the inner curve, hence creating a double spiral. In addition to these passive mechanisms, it is also clear that there is active induction of rotational flow. The left ventricle in the heart twists during contraction which induces a rotational flow component in the aorta. Figure 4.13 shows example of rotational flow observed in different arteries. It has been hypothesised that the presence of rotational flow acts to stabilise flow in the arterial system by reducing shear stress differences (Shipkowitz et al. 2000).

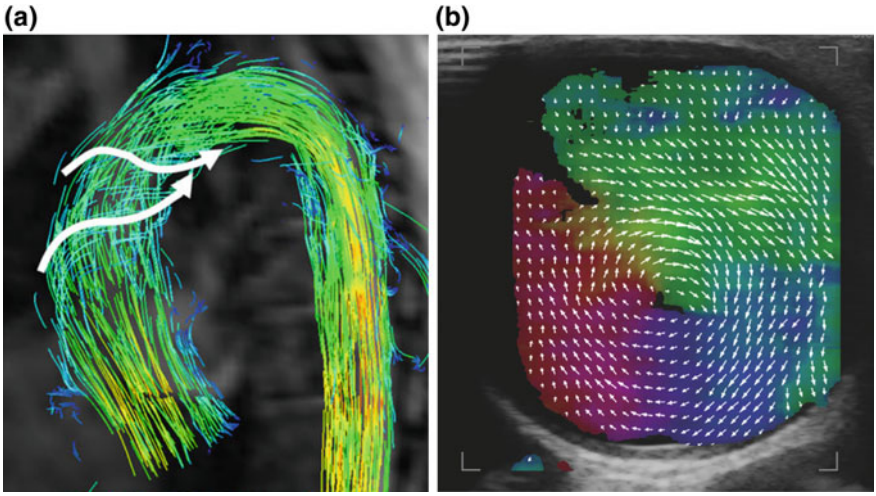

Fig. 4.13 Spiral flow. **a** Typical secondary flow patterns depicted by streamline visualisation in a systolic time frame for the ascending aorta using MRI. **b** Ultrasound colour vector image of spiral flow in the descending aorta. Image (**a**) from European Radiology; Interdependencies of aortic arch secondary flow patterns, geometry, and age analysed by 4-dimensional phase contrast magnetic resonance imaging at 3 T; Vol. 22, 2012, pp. 1122–1130; Frydrychowicz A, Berger A, Munoz Del Rio A, Russe MF, Bock J, Harloff A, Markl M; © European Society of Radiology 2011, with permission of Springer. Image (**b**) provided courtesy of Prof Jensen

Rotational flow also acts to mix blood (Caro et al. 2005; Cookson et al. 2009) which may lead to a more uniform distribution of red cells in arteries. In arteries which are relatively straight and far distant from an upstream branching point it is likely that the rotational component will have diminished and that flow will mainly be axial, for example flow in distal arteries in the legs and arms.

4.3.3 Fully Developed Flow Versus Non-fully Developed

From Chap. 2 the inlet length for flow in a straight pipe is the distance from the inlet beyond which flow is stable ('fully developed'). Under the assumption that the arterial system consists of segments which are straight then the inlet length can be calculated and compared to the length of the segment to get some idea whether flow has any chance of being fully developed. Equation 4.2 is from McDonald (1974, p. 111) and gives the inlet length L_s for the steady-flow component which requires knowledge of the diameter and Reynolds number based on mean velocity through the cardiac cycle.

$$L_s = 0.04d\,Re_{\mathrm{m}} \tag{4.2}$$

The data in Appendix 1 show calculated inlet lengths for steady flow for selected arteries. For the aorta the steady-flow inlet length is greater than the length of the aorta, however, for distal vessels such as the radial and posterior tibial arteries it is less than 2 % of the artery length.

Flow in arteries is pulsatile rather than steady, however as noted by van de Vosse (1998) the pulsatile inlet length is less than the steady-flow inlet length in arteries, so there is no need to consider this. Equations for pulsatile inlet length are provided by Caro et al. (1978, p. 321) and Wood (1999).

On this basis, for most of the larger arteries (aorta, carotid, femoral) flow is not fully developed. For more distal smaller arteries in the leg and arm flow is fully developed, provided it can be assumed that arteries are straight between branching points. This has implications for measurement of flow rate and related quantities using medical imaging where assumptions of fully developed flow are often made (see Chap. 9). The implications are that assumptions of fully developed flow are unlikely to be valid in the larger arteries but may be valid in smaller distal arteries.

4.3.4 Symmetric Versus Asymmetric Velocity Profiles

Velocity profiles in a long straight tube beyond the inlet length are symmetric with respect to the radius. The maximum velocity profile is located centrally within the tube (except in pulsatile flow when the flow passes through zero in which case the maximum velocity is located off-centre). Asymmetric velocity profiles occur when the vessel is curved or immediately downstream of a branching point. In these cases it is necessary to measure the 2D velocity profile. Figure 4.14 shows example of velocity profiles in vivo.

4.3.5 Considerations for Measurement of Blood Velocity and Related Quantities

The above features of blood flow are relevant to estimation of blood velocity profiles using imaging and modelling as will be seen in later chapters. Full 3D flow-field estimation is complex and is generally performed using patient-specific modelling (Chap. 11), though MRI may also provide 3D flow-field data. Simpler methods using ultrasound may rely on assumptions of axial flow for estimation of blood velocity, or on velocity profile symmetry for estimation of flow rate (Chap. 9).

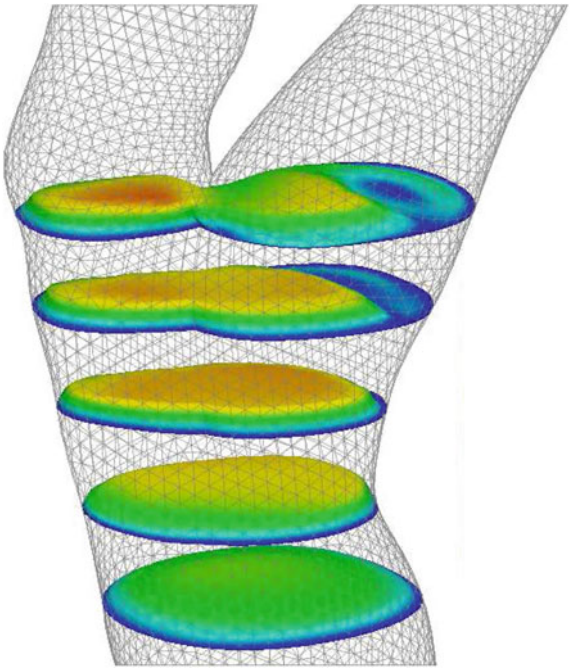

Fig. 4.14 2D velocity profiles in the carotid bifurcation derived from patient-specific modelling. Profiles are symmetric in the common carotid, but asymmetric just below the point of branching and in the internal carotid

Appendix 1: Physical Quantities for Selected Arteries

Data are indicative and taken from various sources including Caro et al. (1978), Marshall et al. (2004) and Reymond et al. (2009). L (length), D (diameter), V_m (mean velocity averaged over time and area), V_p (peak velocity), Re_m (Reynolds number from mean velocity), Re_p (Reynolds number from peak velocity), α (Womersley parameter), L_s (inlet length for the steady-flow component), L_s/L (ratio steady-flow inlet length to arterial length).

	L (cm)	D (cm)	V_m (cm/s)	V_p (cm/s)	Re_m	Re_p	α	L_s (cm)	L_s/L
Descending aorta	21	1.9	22	70	1100	3600	17	86	4.1
Abdominal aorta	13	1.4	13	60	500	2300	15	28	2.1
External iliac/common femoral	14	0.8	16	60	350	1300	5	11	0.8
Superficial femoral/popliteal	44	0.6	15	60	250	1000	4	6	0.1
Posterior tibial	32	0.3	5	50	50	400	3	0.5	0.02
Common carotid	9	0.7	17	80	320	1500	4	9	1.0
Internal carotid	18	0.5	23	75	310	1000	4	6	0.3
External carotid	41	0.4	12	80	130	900	4	2	0.1
Brachiocephalic	42	0.5	8	75	110	1000	8	2	0.1
Radial	24	0.2	5	60	30	300	4	0.2	0.01

References

Caro CG, Cheshire NJ, Watkins N. Preliminary comparative study of small amplitude helical and conventional ePTFE arteriovenous shunts in pigs. J R Soc Interface. 2005;2:261–6.

Caro CG, Pedley TJ, Schroter RC, Seed WA. The mechanics of the circulation. Oxford: Oxford University Press; 1978.

Cookson AN, Doorly DJ, Sherwin SJ. Mixing through stirring of steady flow in small amplitude helical tubes. Ann Biomed Eng. 2009;37:710–21.

Hoskins PR, Fleming A, Stonebridge P, Allan PL, Cameron DC. Scan-plane vector maps and secondary flow motions. Euro J Ultrasound. 1994;1:159–69.

Kilner PJ, Yang GZ, Mohiaddin RH, Firmin DN, Longmore DB. Helical and retrograde secondary flow patterns in the aortic-arch studied by 3-directional magnetic-resonance velocity mapping. Circulation. 1993;88:2235–47.

Marshall I, Papathanasopoulou P, Wartolowska K. Carotid flow rates and flow division at the bifurcation in healthy volunteers. Physiol Meas. 2004;25:691–7.

McDonald DA. Blood flow in arteries. 2nd ed. London: Edward Arnold; 1974.

Murgo JP, Col MC, Westerhof N, et al. Manipulation of ascending aortic pressure and flow waveform reflections with the Valsalva manoeuvre: relationship to input impedance. Circulation. 1981;63:122–32.

Nerem RM, Seed WA, Woods NB. An experimental study of the velocity distribution and transition to turbulence in the aorta. J Fluid Mech. 1972;52:137–60.

Nichols WW, Avolio AP, Kelly RP, O'Rourke MF. Effects of age and hypertension on wave travel and reflections. In: O'Rourke M, Safar M, Dzau V, editors. Arterial vasodilation: mechanisms and therapy. Sevenoaks: Edward Arnold; 1993. p. 23–40.

Reymond P, Merenda F, Perren F, Fenacht DR, Stergiopulos N. Validation of a one-dimensional model of the systemic arterial tree. Am J Physiol Heart Circ Physiol. 2009;297:H208–22.

Roach MR, Burton AC. The reason for the shape of the distensibility curve of arteries. Can J Biochem Physiol. 1957;35:681–90.

Ryan LK, Foster FS. Tissue equivalent vessel phantoms for intravascular ultrasound. Ultrasound Med Biol. 1997;23:261–73.

Shipkowitz T, Rodgers VGJ, Frazin LJ, Chandran KB. Numerical study on the effect of secondary flow in the human aorta on local shear stresses in abdominal aortic branches. J Biomech. 2000;33:717–28.

van de Vosse FN. Cardiovascular fluid mechanics—lecture notes. 1998. http://www.mate.tue.nl/people/vosse/docs/cardio.pdfF

Wood NB. Aspects of fluid dynamics applied to the larger arteries. J Theor Biol. 1999;199:137–61.